

2021-08

High Speed Friction Stir Welding of 5182-H111 Alloy: Temperature and Microstructural Insights into Deformation Mechanisms

Bernard, D

<http://hdl.handle.net/10026.1/15397>

10.1007/s12540-020-00622-y

Metals and Materials International

Springer Science and Business Media LLC

All content in PEARL is protected by copyright law. Author manuscripts are made available in accordance with publisher policies. Please cite only the published version using the details provided on the item record or document. In the absence of an open licence (e.g. Creative Commons), permissions for further reuse of content should be sought from the publisher or author.

High speed friction stir welding of 5182-H111 alloy - temperature and microstructural insights into deformation mechanisms

D Bernard ^{1*}, D G Hattingh ¹, W E Goosen ² and M N James ^{1,3}

¹ Department of Mechanical Engineering, Nelson Mandela University, Port Elizabeth, South Africa

² Centre for High Resolution Transmission Electron Microscopy, Department of Physics, Nelson Mandela University, Port Elizabeth, South Africa

³ School of Engineering, University of Plymouth, Plymouth, England

Abstract:

This paper reports the results of an investigation of thermal cycles and microstructural development in 5182-H111 aluminium alloy during low speed (0.2 m/min) and high speed (1.5 m/min) friction stir welding (FSW), using quenched pin-break specimens. The results show that welds made at both speeds have excellent mechanical properties, although these derive from different thermomechanical mechanisms. For the low speed weld thermal conductivity plays the most significant role in the development of microstructure, while in the case of high speed welding it is the high strain rate plastic deformation that is the dominant mechanism. The yield strength in the stir zone of both the 0.2 m/min and 1.5 m/min welds could be explained through the Hall-Petch relationship, leading to an observable increase in the case of the 1.5 m/min weld. By contrast, an increase in yield strength beneath the shoulder of the 1.5 m/min weld was driven by strain hardening.

Keywords:

High speed FSW; 5182-H111 alloy; thermal cycles; pin-break; slip systems

* Corresponding author dreyer.bernard@mandela.ac.za

1. Introduction

Although high welding speeds can be readily attained in MIG welding of 5xxx and 6xxx aluminium alloys, e.g. reference [1] that reports welding speeds of 2.5 m/min and 3.5 m/min in 4 mm thick 6061-T6 aluminium alloy, it has proven harder to obtain high speeds in friction stir welding (FSW) whilst maintaining high levels of mechanical properties. Relatively few papers have therefore dealt with high speed welding of 5xxx alloys, despite its high industrial desirability. Rodrigues et al [2] compared the friction stir (FS) weldability of two commonly used structural aluminium alloys, 5083-H111 and 6082-T6 in 4 mm and 6 mm thick plates, obtaining speeds in the range 0.35 m/min to 0.5 m/min in the 5083 alloy. They also reported high levels of joint efficiency with matched yield strength values and elongation ratios (calculated as the ratio between the elongation of the weld samples and parent plate at maximum load) as high as 0.8 in the 4 mm plate and perhaps 0.75 in the 6 mm plate. In the 6082 alloy, they obtained higher welding speeds of up to 1.1 m/min for the 3 mm plate. Ericsson and Sandström [3] have also performed work on 6082 alloy where FSW speeds of 0.7 m/min and 1.4 m/min were used in 4 mm plate. Their results indicated that, for this heat treatable alloy, the FSW welding speed had little discernible difference on the tensile properties of the welds, provided that a post-weld aging heat treatment was carried out. This gave joint efficiencies in the T4 condition close to 1.0. They noted however, that the lower welding speed led to an increased fatigue performance possibly due to the increased heat input per unit length of the weld.

The main issue in achieving high FSW speeds in 5xxx alloys arises from the fact that they are primarily strain-hardening alloys and FSW is a thermomechanical solid-state process in which significant strain-induced microstructural changes occur causing

dynamic recrystallisation in the weld nugget stir zone (SZ) along with very significant plastic deformation and strain rates in the thermomechanically-affected zone (TMAZ). There is clearly considerable scope for altering the microstructure in terms of grain size, precipitation and dislocation structures across the weld zone. In principle, therefore, there is a significant opportunity to tailor the process parameters to achieve useful combinations of high process speeds and high mechanical performance.

At present, there is relatively little published work on FSW of 5xxx alloys that has considered high welding speeds (i.e. ~1.5 m/min) and their influence on microstructure and hence on mechanical properties in the weld zone. A previous publication by Bernard and Hattingh [4] has briefly reported the development of process parameters that can achieve void-free FS welds made at 1.5 m/min (25 mm/s) and at 0.20 m/min (3.33 mm/s) in 5 mm thick 5182-H111 plate. These parameters gave a strain to failure that was 91% of the parent plate and had a tensile joint efficiency > 1.0.

As noted by Prangnell and Heason in reference [5], the large majority of studies of grain structure obtained during FSW derive from studies of completed welds, and the additional information obtained from freezing the welding process by rapidly arresting tool motion and quenching the specimen offers significant additional insights into microstructural interpretation. This is the area of interest in the work reported in this paper.

Microstructural Development in FS welded 5xxx Alloys

A significant body of work now exists dealing with microstructural evolution during FSW although, as noted by Tronci et al [6], FSW of 5xxx alloys is perhaps less well

explored than is the case for the heat-treatable 2xxx, 6xxx or 7xxx alloys. Tronci et al [6] conclude from their review of the available literature that the mechanical properties of FS welds in 5xxx alloys depend mainly on the grain size, dislocation density due to plastic deformation, and recrystallisation during welding. They further observe that annealed alloys in the 5xxx-O condition do not experience softening in the TMAZ or heat-affected zone (HAZ) regions of the weld. In contrast when a strain hardened temper (i.e. H321) is welded the thermal cycles and large plastic strains result in softening through recovery and static or dynamic recrystallisation.

McNelley, Swaminathan and Su have discussed dynamic recovery and recrystallisation mechanisms during FSW of aluminium alloys in a recent paper [7] noting that heating is due to a combination of friction effects and severe, localised, adiabatic deformation induced in the material by tool rotation. The heat source is therefore distributed in a volume of deforming material surrounding the pin. This volume of material is usually referred to as the weld nugget or stir zone (SZ).

Three distinct weld regions can be recognised in FS welds and these are characterised by McNelley et al [7] as: the weld nugget or SZ where large plastic strains occur at strain rates in the range 10^1 to 10^2 s⁻¹ and where peak temperatures are in the range 0.6 to 0.95 T_{melt} , depending on the alloy, tool geometry and process parameters. The region of the SZ immediately under the tool shoulder experiences additional heating and deformation from shoulder contact. The TMAZ experiences lower temperatures, lower strain and lower strain rates. It is usually characterised by a pattern of grain distortion that reflects shearing and material flow around the rotating tool. Grain distortion near the interface between the SZ and the TMAZ may lead to the formation

of refined equiaxed grains. The HAZ lies beyond the TMAZ and is a region where the material has experienced a purely thermal cycle.

Strain hardening aluminium alloys like 5182 can be FS welded to provide fully efficient joints in tensile property terms, through appropriate choice of process parameters that lead to appropriate combinations of strain hardening and other strengthening mechanisms, as discussed above. Dynamic recovery (DRV) occurs readily during hot working of aluminium which has a high stacking fault energy. During FSW the flow stress initially rises as dislocations multiply and interact [7]. However, the rate of recovery also increases as the dislocation density increases and hence dislocations begin to rearrange and form low-angle boundaries as subgrains develop. The flow stress eventually saturates as dislocation multiplication and recovery due to this rearrangement reaches a dynamic equilibrium. This steady state is reflected in equiaxed subgrains with nearly dislocation-free interiors, with fairly constant subgrain size and boundary misorientation.

The work by Tronci et al [6] considered 1 mm plate of 5182-H111 and 5083-H111 alloys and concluded that for 5182-H111 welds, the TMAZ subgrain structure played a major role in determining mechanical properties, with lower grain sizes resulting from lower temperature welding and larger grain sizes from higher welding temperatures. They also observed a higher grain size variation with the lower welding temperatures (corresponding with low ratios of tool rotational speed over transverse welding speed, equivalent to the inverse of weld pitch in Table 2). A strong Hall-Petch relationship existed for the 5182 alloy between the grain size in the TMAZ and the hardness, ranging from matched hardness with the parent plate at larger grain sizes (lower

traverse speeds) to overmatched hardness values at smaller grain sizes (higher traverse speeds and reduced heat input) [6].

The work described in this paper falls into two parts and utilised the process parameters for successful FS welding at 0.2 m/min and 1.5 m/min discussed in previous work performed by Bernard and Hattingh [4]. In the first part, the previous work has been extended by discussing the heat flow and temperature profiles measured during welding at these two feed rates, and relating them to the resulting microstructure and local mechanical properties. The second part provides a qualitative overview of the microstructural development during welding, aimed at giving insight into the different deformation mechanisms that occur during slow and fast welding. This part of the work applied a weld microstructure freezing (stop-action) technique [5, 8] to investigate the development of the microstructure immediately ahead of the approaching weld tool and to examine the microstructural development that contributes to yield strength, particularly in the stir zone (SZ).

2. Experimental Procedure

Material and Welding Parameters

The 5182-H111 aluminium (supplied as Hulamin T500 tanker plate) used in this work is a non-heat treatable, strain hardening alloy used for the fabrication of ground vehicles, particularly road tankers, because of its favourable combination of good formability, very good resistance to corrosion and high tensile elongation. Plate with a nominal thickness of 5.15 mm was used in this work with the composition given in Table 1.

In the weld trials reported in reference [4], successful high integrity welds could be achieved with feed rates of 1.5 m/min (25 mm/s) and 0.2 m/min using a spindle speed of 500 rev/min. Using a single spindle speed gives a useful basis for comparing the differences in microstructural development during these trials. The weld process parameters used in both the previous study and the present one are given in Table 2. The high speed welds (1.5 m/min) made using these parameters overmatched the tensile properties of the parent plate, achieving a mechanical joint efficiency (ratio of tensile strengths) of 1.04, a 0.2% proof strength ratio of 1.22 while the percentage elongation at fracture was 91% of that achieved by the parent plate. The low speed welds made at 0.2 m/min achieved ratios for the equivalent parameters of 1.03, 1.05 and 1.04. Table 3 compares the mechanical properties of the successful low and high speed welds with those of the 5182 H-111 parent plate. The tensile samples (which had a width and thickness of 12.5 mm and 5.15 mm in accordance with ASTM E8M) were sectioned longitudinally from the weld zone, and therefore consisted entirely of weld metal.

The process parameters given in Table 2 were used in both parts of the present work with all welds made using an MTS I-stir friction process development platform. For the first part of the work butt welds were made between plates with a length of 500 mm and a width of 135 mm. The threaded conical pin tapered from 10 mm diameter to 8 mm diameter, and had 3 equispaced flutes. The tool was manufactured from W302 Böhler hot work die steel hardened to 54 HRC, with a shoulder diameter of 22 mm and welds were made with a forwards tool tilt of 2°. The weld process was carried out in force control, with forging forces given in Table 2.

In the second part of the work dealing with the stop-action, or “pin-break” welds, central bead-on-plate welds were made in position control using a flute-less tool with all other dimensions remaining the same as in the first part. Position control was used because sudden pin failure in force control mode could have caused significant machine damage due to the high forces associated with the 1.5 m/min weld.

The pin was notched at its base to achieve a controlled break during welding in a similar fashion to the work by Chen, Pasang and Qi [9]. Immediately on failure, the weld zone was quenched with water to 'freeze in' the microstructure around the tool. Weld cooling rates were monitored as $\approx 150^{\circ}\text{C/s}$ over the critical range between circa 420°C and $<100^{\circ}\text{C}$. The weld coupons were used for microstructural evaluation only if the pin break occurred once the welding conditions had fully stabilised, i.e. after a welding length of typically 130 mm. The weld was then sectioned along its horizontal plane with the tool pin still in place, and EBSD microstructural analysis was performed ahead of the leading edge of the pin. Note that all welds were made perpendicular to the rolling direction in the aluminium plate.

Microstructural sample preparation and analysis

For the first part of the work, the cross-sectional microstructure was prepared by mechanical polishing to a final finish of $0.04\ \mu\text{m}$ colloidal silica suspension, followed by electrolytic etching with Barker's reagent (4 ml Fluoroboric acid in 200 ml H_2O) for analysis by polarized light. The electron backscatter diffraction (EBSD) work involved mechanical polishing with colloidal silica to a $0.04\ \mu\text{m}$ finish.

In the second part of the work dealing with stop-action welds, microstructural evaluation was performed on a plane parallel with the specimen surface (RD-TD in Figure 1) at a depth of 1.7 mm. In addition, one specimen at both welding speeds was sectioned along the weld in the (TD-ND) plane through the centre of the pin. Sample preparation for light microscopy involved mechanical polishing to a 0.04 μm finish with colloidal silica suspension and etching with a solution of 1% NaOH in H₂O for macrographic analysis. Electrolytic etching with Barker's reagent was again used for microstructural analysis under polarized light. The EBSD work was performed on the surface that had been mechanically polished with colloidal silica.

EBSD work used a JEOL JSM 7001F FEG SEM fitted with a Nordlys EBSD detector, and an electron beam accelerating voltage of 15 kV. A step size of 0.02 μm was used for the EBSD scans in front of the tool for both welds, while 0.5 μm and 0.3 μm were respectively used for the advancing and retreating side scans of the slow and fast speed welds. In the EBSD analysis a grain boundary misorientation $>10^\circ$ was defined as a high angle boundary (HAGB), while $<10^\circ$ was defined as low angle boundaries (LAGB) or sub-grain boundaries. Figure 1 shows the sample orientation in EBSD terms used in this work.

In the work on stop-action welds, the microstructural changes ahead of the leading edge of the tool pin were characterised in the following manner. The region ahead of the welds was divided into rectangles 128 μm x 80 μm , and the average grain size in each area was found as the diameter of an equivalent circle. Grain size density was then defined as the number of grains of a particular size category per 100 μm^2 in a particular area, using convenient grain size ranges, namely 0-2 μm , 2-4 μm , 4-10 μm ,

10-15 μm and $>15 \mu\text{m}$. This allowed direct grain size comparison between different areas as well as between the slow and fast welds.

The extent of deformation was analysed via plots of the recrystallized fraction component and local misorientation, and also by plotting the low angle (LA) and high angle (HA) grain boundary frequency and density as functions of distance ahead of the tool. The recrystallized fraction component was determined using Channel 5 software, which considers the grain average misorientation (GAM). The grains are reconstructed considering low angle grain boundaries (LAGB) between 1° and 7.5° , and high angle grain boundaries (HAGB) above 7.5° . A measure of the average internal grain orientation is then determined, and each grain is coloured in accordance with its average sub-grain misorientation. Recrystallized grains are considered as having an average subgrain misorientation of less than 1° , and are shown in blue. Substructured grains (which are recrystallized grains with subgrains) have an average misorientation between 1° and 7.5° , and are identified in yellow. Deformed grains are red, and are grains with an average misorientation higher than 7.5° . The level of subgrain misorientation is also presented as a "grain boundary frequency", which was obtained using lines drawn parallel to the welding direction and is defined as the number of LA and HA grain boundary intercepts/100 μm of line.

3. Results: Part 1

3.1 Measurement of thermal cycles

Temperature data measured during the previous work described in reference [8] on low and high speed welds are presented here. Temperature data were recorded in two ways. Firstly thermocouples were embedded within the work-piece. These

thermocouples were embedded at the mid-thickness of the plate (i.e. 2.5 mm), on both the retreating and advancing sides of the weld. The thermocouples had transverse offsets from the weld centreline of 13 mm, 18 mm and 23 mm, as illustrated in Figure 2a. Two additional thermocouples were also placed 10 mm further along the weld, and were angled relative to the top surface (Figure 2a). These thermocouples were initially located 5.5 mm either side of the centreline and were displaced by plastic deformation during welding (indicated with the red arrow in Figure 2a) and their measurements were therefore taken as corresponding with the final thermocouple position. Repeat welds indicated that the measurements with the displaced position were repeatable, and they are therefore taken as representative. Secondly a thermocouple was embedded within the pin of the rotating FSW tool, and the measurements were transmitted through wireless telemetry. Figure 2b shows an image of the various thermocouples mounted in position in the plate after welding, while Figure 2c shows an illustration of the thermocouple embedded within the pin. Repeatable measurements of peak temperatures were achieved using this method.

The temperature contour plots in Figures 3a and 3b are a function of transverse distance from the weld centreline (y-axis) and the time over which a particular temperature was maintained relative to the centreline (x-axis) of the tool as it passed the measurement position. Figures 3c and 3d give the peak temperature measurements as a function of the transverse distance from the tool centreline, with negative distances representing distance ahead of the tool. This representation illustrates the very confined time and sharp rise-time associated with peak weld temperatures at any point in the weld run during high speed welding. Clearly this

would have a significant impact on the weld microstructure and hence on the weld properties.

The individual peak temperature measurements recorded at each thermocouple for the FS welds are shown in Figure 4. Negative distances represent the retreating side while positive values represent the advancing side of the weld. The peak temperatures within the tool pin were measured using wireless telemetry and an embedded thermocouple, positioned approximately 0.5 mm from the tool side at the mid-depth of the weld. Peak temperatures of 543°C in the 0.2 m/min weld and 505°C in the 1.5 m/min weld were recorded and confirmed for three welds at each welding speed.

In considering the thermomechanical deformation mechanisms relevant to low and high speed FS welds, work by Hamasaki, Morimitsu and Yoshida [10] on 5182-O alloy has indicated that at a temperature of 200°C the flow stress shows a significant drop compared with lower temperatures, and a significant strain rate dependence of flow stress was also observed at this temperature. This observation is supported in other work on 5182 alloy reported by Chen et al [11], while Park et al [12] in work on 5083 alloy state that recovery was observed in severely plastically deformed alloy at temperatures of approximately 200°C. Considering the low speed FSW data in Figure 3c (specimen welded at 0.2 m/s or 3.3 mm/s) a temperature of 200°C is reached 4.5s (15 mm) before the tool centre reaches the closest thermocouples and decays below 200°C 10.6s after the tool centre has passed this position. The peak recorded temperature of 480°C for the closest thermocouples (6.5 mm from the tool centreline) is reached at almost the same time as the tool centre passed by this this thermocouple.

In contrast, for the high speed specimen welded at 1.5 m/min or 25 mm/s, Figure 3d shows that the corresponding times during which a temperature of 200°C is reached 0.20s before the tool centre reaches the closest thermocouples (4.5 mm from the tool centreline) and the temperature exceeds 200°C for a total of 2.6s. The peak recorded temperature for the closest thermocouple of 421°C is reached 0.2s after the tool centre has passed by the thermocouple.

The data in Figure 3 can therefore be interpreted in the following manner. Figures 3a and 3c indicate that during slow FSW, heating commences through conduction well in advance of the arrival of the tool shoulder, reaching a temperature of $\approx 250^\circ\text{C}$ by the time it reaches the thermocouple position ($\approx 400^\circ\text{C}$ by the time the pin passes the thermocouple). This correlates with the conventional description of heat generation in FSW, e.g. [13], where frictional stress at the tool-workpiece interface determines the temperature profile and plastic deformation around the tool. However, in the case of the fast FSW at 1.5 m/min, the temperature profiles in Figures 3b and 3d indicate that a temperature of $\approx 200^\circ\text{C}$ is reached at approximately the same time that tool pin arrives at the thermocouple located closest to the weld centreline. This is interpreted as showing that the travel speed of the tool exceeds the rate at which heat is conducted through the alloy ahead of the tool and hence there should be very little reduction in the flow stress before the tool pin arrives to stir the material. There are two competing influences on the flow strength during welding, namely the conduction time and the strain rate. In this context, Higashi et al [14] in high strain rate work ($10^{-3}/\text{s}$ to $4 \times 10^3/\text{s}$) on aluminium alloys, found that for 5182 alloy at room temperature the maximum flow stress decreased with increasing strain rate in the range $10^{-3}/\text{s}$ to $10^2/\text{s}$.

They also observed that there was a greater reduction in flow stress in the low ($10^{-3}/s$ to $10^{-1}/s$) and intermediate range of strain rates ($10^{-1}/s$ to $3 \times 10^2/s$) with increasing Mg content in the aluminium alloys. Presumably this trend of reduction in flow stress would be enhanced at higher temperatures, as observed at lower strain rates by Jang and Kim [15] who, in tests at temperatures of $150^{\circ}C$ to $450^{\circ}C$, observed a reduction in flow stress from approximately 270 MPa to 56 MPa at a strain rate of $10^{-1}/s$ and 230 MPa to 7 MPa at $5 \times 10^{-4}/s$.

In summary, the data in Figure 3 together with references [10, 12, 14] indicate that the mechanisms underlying the required thermomechanical deformation during high and low speed FSW are likely to be different, with the reduction in flow stress during welding having a stronger conduction-induced component in low speed FSW and reflecting the greatly increased strain rate in the case of high speed FSW.

3.2 Local mechanical properties and microstructure

The micrographs for the 0.2 m/min and 1.5 m/min welds are respectively shown in Figures 5 and 6. EBSD recrystallized fraction plots are given for the slow speed weld in Figures 5b to 5f and for the high speed weld in Figures 6b to 6f. The microstructure of FS welded 5xxx-series alloys in the H111 strain temper does not show a clear HAZ zone since the heat associated with the process does not cause observable grain growth. The weld cross section is divided into the following zones as shown in Figures 5a and 6a. These zones are described as follows; the stir zone (SZ) consisting entirely of dynamically recrystallized grains, stir zone plus thermomechanically affected zone (SZ + TMAZ) which describes the highly deformed region immediately adjacent to the SZ, the thermomechanically affected zone (TMAZ) which is directly beneath the

shoulder, and the HAZ which is considered to occur immediately outside the shoulder since it is not possible to clearly identify this zone. In Figures 5 and 6, (a) illustrates the recrystallized fraction component of the SZ, (b) and (c) the HAZ on the retreating and advancing sides respectively, and (e) and (f) show an area extending from the TMAZ+SZ, into the SZ on the retreating and advancing sides respectively. Also shown in Figure 7 are the area fractions of recrystallized, substructured and deformed grains for the 0.2 m/min and 1.5 m/min weld.

For the 0.2 m/min weld, the stir zone is characterized by mainly recrystallized ($<1^\circ$ misorientation) and moderately deformed grains (misorientation between $1^\circ - 7.5^\circ$), with an average grain size of $9.7 \mu\text{m}$, compared to the initial average parent grain size of $15 \mu\text{m}$. The TMAZ, which in the case of the 0.2 m/min weld experiences predominantly thermal cycle without any significant plastic strain, is characterized by an average grain size of $15 \mu\text{m}$, which comprise either recrystallized grains (blue) or subgrains (yellow). From Figure 7 the SZ contains almost no deformed grains, while the TMAZ contains 76% and 82% substructured, 10% and 8% recrystallized and 13% and 10% deformed grains on the retreating and advancing sides respectively. In contrast, the 1.5 m/min weld had a smaller grain size of $4.9 \mu\text{m}$ in the stir zone, again comprising primarily recrystallized or moderately strained grains. The grains in the TMAZ, however, which also had an average grain size of $14 - 15 \mu\text{m}$, were characterized either by subgrains or deformed grains (misorientation $>7.5^\circ$). Figure 7 shows that the SZ of the 1.5 m/min weld comprises 25% recrystallized, 60% substructured and 15% deformed grains, while the TMAZ contained 13% and 9% recrystallized, 70% and 63% substructured and 17% and 28% deformed grains for the retreating and advancing sides of the TMAZ respectively.

The 1.5 m/min weld displays a higher percentage of deformed grains at all the positions sampled, with an observable amount of deformed grains in the SZ. The TMAZ on both the retreating and advancing sides contained higher percentages of both deformed and recrystallized grains. This deformation in the 1.5 m/min weld is caused by the high stress beneath the shoulder arising from the forging force of 59 kN. Though not as severe as in the TMAZ+SZ, the volume of material beneath the shoulder clearly experienced a degree of deformation in the 1.5 m/min weld.

The local mechanical properties for the 0.2 m/min and 1.5 m/min welds were determined by removing small section tensile specimens longitudinally with a width and thickness of 3 mm and 1 mm respectively. The sample geometry and their location across the weld is indicated in Figure 8. Twelve such samples were cut from each weld, with a pitch of approximately 1.5 mm between each specimen, however, only one sample from each position was tested. The position of the tensile samples in the weld was verified by etching the grip cross-section after the test (Figure 8b). The red dots show the samples that were tested to ensure that the complete cross-section was in the appropriate part of the weld zone.

Figures 9a and 9b show the variation in the ultimate tensile strength (UTS) and yield strength across the weld zone, while the corresponding Hall-Petch relationship is plotted in Figure 10 for the SZ and TMAZ regions. The yield strength of AA5182 is affected by grain size, solid solution strengthening and precipitate strengthening. The Hall-Petch relationship (which considers the effect of grain size) adequately describes the proof strength behaviour for the stir zone and TMAZ of the 0.2 m/min weld and the

stir zone of the 1.5 m/min, confirming that the strength difference between these areas is primarily due to the differences in grain size. However, the TMAZ data for the 1.5 m/min weld (green circles) do not fit this relationship. The position where each sample was removed is illustrated in Figure 9, where the microstructural macrographs are scaled in accordance with the x-axis. The tensile samples from the 1.5 m/min weld that deviated from the Hall-Petch relationship (-11.2 mm, -8.3 mm, +8.4 mm, +11.3 mm) all originated from the TMAZ. The highest yield stress was attained by the sample from the TMAZ+SZ on the retreating side of the 1.5 m/min weld, however, due to the complex and inhomogeneous strain and grain size characteristics associated with this zone, the TMAZ+SZ sample is not represented on the Hall-Petch plot. As illustrated in Figure 7, the TMAZ displayed a higher area fraction of deformed grains in the 1.5 m/min weld, and the TMAZ+SZ shown in Figure 7e experienced severe plastic strain. The improved TMAZ yield strength, relative to the Hall-Petch relationship cannot, therefore, be attributed to grain size alone. Since this region also experiences limited thermal exposure, the precipitate distribution will not alter, and no solute strengthening elements (magnesium) can diffuse from the matrix. Thus, the strength increase is attributed to the strain hardening due to the high tool forging force of 59 kN and the associated very short thermal cycles, as discussed in the previous section.

4. Results: Part 2

Stop-action experiments

In the case of the high speed welds, the confined thermal exposure clearly limits recovery and grain growth during the cooling cycle, and in order to better understand the preceding deformation and recrystallization mechanisms leading to the refined

grain size in the 1.5 m/min welds, stop-action experiments were carried out using a simplified flute-less pin design.

Figure 11 shows cross sectional macrographs of the pin-break welds made at 0.2 m/min (Figure 11a) and 1.5 m/min (Figure 11b). Both welds are fully consolidated therefore considered valid for use in this investigation. Shown in Figures 12 and 13 are the side view (plane TD – ND) and top view (plane TD – RD) of the stop action experiments for the 0.2 m/min and 1.5 m/min welds respectively. The deformation characteristics will now be discussed in the rectangular region ahead of the tool in Figures 12b and 13b marked '1'. The position of the horizontal plane is also illustrated by the red lines marked '1' in Figures 12a and 13a.

Figures 14 and 16 presents the recrystallized fraction component (GAM) for the area 'a' as illustrated in Figures 12b and 13b respectively representing the 0.2 m/min and 1.5 m/min welds. This area was broken into visually consistent zones as observed from the recrystallized fraction component. Since these zones were all of different size, the grain size is reported as a grain density, while the grain boundary frequency is presented as intercepts per 100 μm . This allowed areas of different sized and from different welds to be compared. The prefix "S" or "F" on each zone distinguishes the "slow" (0.2 m/min) and "fast" (1.5 m/min) welds.

4.1 EBSD recrystallisation data for the low speed (0.2 m/min) weld

Figure 14 shows the EBSD recrystallized fraction plot ahead of the tool pin (indicated by negative distances) for the 0.2 m/min weld on the TD-RD plane (see Figure 1) at a depth of 1.7 mm below the weld surface. Blue regions indicate recrystallized grains,

yellow indicates substructured grains and red indicates deformed grains. In the first 0.5 mm ahead of the tool pin, the majority of the grains are recrystallized, while the proportion of deformed regions steadily increases between 0.8 mm and 2.1 mm ahead of the pin. Dynamically recrystallized grains initiate on HAGB's and are initially small with low aspect ratios. As dynamic recrystallisation progresses the average HA grain size is reduced and the frequency of smaller grains increases. This sequence of events can be seen unfolding in the region that commences about 1.35 mm ahead of the pin and it steadily continues as the pin approaches. Similarly, during grain growth the average grain size will increase in relation to the number of grains that have reduced in size and this phenomenon can be observed occurring in the final 0.5 mm ahead of the pin. Grain deformation due to plastic deformation is indicated by their aspect ratio, with more highly deformed grains having higher aspect ratios and this is evident in the region 2.1 mm to 1.25 mm ahead of the pin.

Figure 15 illustrates microstructural evolution in terms of changes in grain misorientation obtained via data for grain boundary frequency (Figure 15a) and grain size density (Figure 15b) ahead of the tool for the low speed (0.2 /min) weld. In zone S-4, following an initial decrease in grain boundary intercepts between 2.1 mm ahead of the pin and ≈ 1.8 mm, there is a subsequent increase to 1.4 mm from the pin. There is an associated initial increase in average equivalent grain diameter, followed by a decrease from about 13 μm at 1.8 mm from the pin to around 11 μm 1.4 mm ahead of the tool. In zone S-3 and S-2, a steady increase in grain boundary intercepts occurs to 0.6 mm ahead of the pin, followed by stability between approximately 0.6 mm and 0.4 mm ahead of the pin and then a decline as the pin approaches. LAGB intercepts are reasonably constant until approximately 0.9 mm ahead of the pin after which they decrease steadily but with a decreasing gradient. HAGB intercepts

increase marginally over both zones, while the average grain size intercepts decrease to 0.8 mm ahead of the pin and then remain constant in zone S-1. These trends reflect the onset of recrystallisation as plastic deformation increases as the weld moves towards the pin through zones S-4 to S-1 [7]. This is supported by the increase in the density of 2 - 4 μm and particularly 4 - 10 μm grains over the same regions in Figure 15b. In region S-1 the average grain size shows a marginal increase, driven largely by a strong increase in density of 4 - 10 μm grains and a slight increase in density of 10 - 15 μm grains (Figure 15b). This latter increase for the larger diameter grains occurs due to associated growth of newly recrystallized grains driven by the elevated temperature (see Figure 3c). The reduction in the frequency of LAGB from about 0.9 mm in front of the pin is evidence of dynamic recrystallization. In zone S-1 a reasonably stable relationship between LA and HA grains is seen, along with a fairly constant average grain size reflecting dynamic recrystallisation as the highly deformed alloy is extruded around the pin.

4.2 EBSD recrystallisation data for the high speed (1.5 m/min) weld

The recrystallisation mechanisms occurring in the high speed weld were more complex, reflecting the limited extent of conduction heating ahead of the tool seen in Figure 3b and the increased role of high strain rate plastic deformation in the welding process. The recrystallized grain fraction as a function of distance ahead of the pin is shown in Figure 16, while Figure 17 gives grain boundary intercept frequency and grain density information. Figure 16 demonstrates a much higher incidence of highly strained grains (red) in the region from approximately 1.2 mm ahead of the pin compared with Figure 14, reflecting the high levels of plastic deformation and limited thermal conduction involved in high speed FS welding. Significant but well dispersed recrystallisation (blue) therefore also occurs in the high speed weld in the region

closer than 1.2 mm ahead of the pin. Some grains showed evidence of strain driven recrystallization through grain sub-division. The recrystallized fraction component (GAM) and local misorientation plot (KAM) for a grain 1.95 mm ahead of the tool in the 1.5 m/min weld are shown in Figure 18. In face-centred crystal structures slip occurs primarily on the {111} plane, along the $\langle 100 \rangle$ direction. When a grain is favourably oriented for five slip systems to be activated from the deformation field generated by the pin, geometrically necessary boundaries (GNB's) will form along the {111} planes. According to Kaibyshev and Malopheyev [16] GNB's form along the most stressed {111} planes owing to high strain gradients within narrow zones of plastic deformation due to simple shear. They observe that this mechanism can lead to an ultra-fine grained (UFG) structure in aluminium alloys. In the grain shown in Figure 18, evidence of possible grain subdivision is seen in the high subgrain misorientation (approximately 5° as circled in the misorientation plot) is aligned nearly perpendicular to the welding direction (the solid black line in the figure).

Figure 17a shows that in zone F-4 (in the region between 1.6 mm and 0.9 mm ahead of the pin) there is an increase in the number of grain boundary intercepts per 100 μm for both LA and HA grains, with the increase being particularly marked for LA grains. There is therefore a concomitant decrease in overall grain diameter in zone F-4 and, as seen in Figure 17b, a large increase in the number of very small grains in the range 0 - 2 μm as well as an increase in the density of grains in the range 2 - 4 μm . This shows clearly that recrystallisation is occurring and leading to decoration of HAGB's with recrystallized grains, as can be observed in Figure 16 in this region. Within a distance of 0.6 mm ahead of the pin, the grain density of these two LA grain size ranges increases even more markedly. The density of 4 - 10 μm grains also

increase sharply from a point 0.6 mm ahead of the pin, before declining again at approximately 0.2 mm in front of the pin.

Figure 17a shows that the number of HAGB intercepts increases from a point 0.4 mm ahead of the pin, with the increase becoming even greater from 0.2 mm ahead of the pin. In other words, and as seen in Figure 16, the formation of new recrystallized HA grains increases from a point approximately 0.4 mm ahead of the pin and they form the bulk of the microstructure from a point 0.2 mm ahead of the pin. The recrystallized regions are more uniformly distributed in the case of high speed FS welding than they are for low speed welding (Figure 14).

5. Conclusions

This work has presented information on the thermal cycles, mechanical properties and microstructure obtained during low (0.2 m/min) and high speed (1.5 m/min) FSW of 5182-H1111 aluminium alloy. “Pin-break” (stop-action) welds were quenched in order to examine the microstructural development ahead of the tool pin during the welding process using EBSD. The following conclusions can be drawn:

1. In FS welding at 0.2 m/min (0.4 mm/rev) a temperature of 200°C is reached some 4.5s (15 mm) in advance of the arrival of the pin, and remains above 200°C for 10.6s. In contrast, in welding at 1.5 m/min (3 mm/rev), this temperature is only reached approximately 0.20s in advance of the pin, and is only exposed to temperatures exceeding 200°C for 2.6s
2. The increased yield strength in the SZ of the 1.5 m/min weld is a result of grain refinement, indicated by the Hall-Petch relationship. The increase in the yield strength

beneath the shoulder of the 1.5 m/min weld (TMAZ) is attributed to strain hardening due to the high forging force of 59 kN.

3. The mechanisms involved in lowering the flow stress and developing the microstructure in the TMAZ and SZ are hence very different at the two welding speeds, having a large conduction component in low speed welding and a high strain rate component in high speed welding. This change in mechanism has a very significant effect on the weld microstructure in the TMAZ and the stir zone (SZ).

Recrystallisation plots obtained from the pin-break and stop-freeze experiments are very different at low and high welding speeds. The high speed weld shows a much greater incidence of highly strained grains commencing approximately 1.2 mm ahead to the pin and associated high levels of well dispersed dynamic recrystallisation. Within a distance of 0.6 mm ahead of the pin the microstructure is very largely recrystallized with a very fine grain size, which increases the proof strength by 22% compared with the parent plate and 15.6% compared with the low speed weld.

Acknowledgements

The authors acknowledge the funding support provided by Advanced Metals Initiative (Light Metals Development Network) of the Department of Science & Technology, Republic of South Africa, the National research Foundation (NRF) and the German Academic Exchange Service (DAAD) for Dreyer Bernard.

References

1. Horita M, Makita S, Hori H, Hino H. Development of high-speed MIG welding process. First report: Arc phenomena and formation mechanisms of surface defects. *Welding International*. 1999;13(4):270-5.

2. Rodrigues DM, Leitão C, Louro R, Gouveia H, Loureiro A. High speed friction stir welding of aluminium alloys. *Science and Technology of Welding and Joining*. 2013;15(8):676-81.
3. Ericsson M, Sandström R. Influence of welding speed on the fatigue of friction stir welds, and comparison with MIG and TIG. *International Journal of Fatigue*. 2003;25(12):1379-87.
4. Bernard D, Hattingh DG. Development of High Welding Speed in Friction Stir Welded 5182-H111, and the Resulting Influence on down Force. *Materials Science Forum*. 2015;828-829:366-73.
5. Prangnell PB, Heason CP. Grain structure formation during friction stir welding observed by the 'stop action technique'. *Acta Materialia*. 2005;53(11):3179-92.
6. Tronci A, McKenzie R, Leal RM, Rodrigues DM. Microstructural and mechanical characterisation of 5XXX-H111 friction stir welded tailored blanks. *Science and Technology of Welding and Joining*. 2013;16(5):433-9.
7. McNelley TR, Swaminathan S, Su JQ. Recrystallization mechanisms during friction stir welding/processing of aluminum alloys. *Scripta Materialia*. 2008;58(5):349-54.
8. Fonda RW, Knipling KE, Bingert JF. Microstructural evolution ahead of the tool in aluminum friction stir welds. *Scripta Materialia*. 2008;58(5):343-8.
9. Chen ZW, Pasang T, Qi Y. Shear flow and formation of Nugget zone during friction stir welding of aluminium alloy 5083-O. *Materials Science and Engineering: A*. 2008;474(1-2):312-6.
10. Hamasaki H, Morimitsu Y, Yoshida F. Stress relaxation of AA5182-O aluminum alloy sheet at warm temperature. *Procedia Engineering*. 2017;207:2405-10.
11. Chen SR, Stout MG, Kocks UF, MacEwen SR, Beaudoin AJ, editors. Constitutive modelling of a 5182 aluminium as a function of strain rate and temperature. *Hot Deformation of Aluminium Alloys II*; 1998; Rosemont, Illinois: TMS.
12. Park K-T, Hwang D-Y, Chang S-Y, Shin DH. Low-temperature superplastic behavior of a submicrometer-grained 5083 Al alloy fabricated by severe plastic deformation. *Metallurgical and Materials Transactions A*. 2002;33A(September 2002):2859-67.
13. Sun Z, Wu CS, Kumar S. Determination of heat generation by correlating the interfacial friction stress with temperature in friction stir welding. *Journal of Manufacturing Processes*. 2018;31:801-11.
14. Higashi K, Mukai T, Kaizu K, Tsuchida S, Tanimura S. Strain rate dependence of on mechanical properties in some commercial aluminum alloys. *Journal de Physique IV Colloque*. 1991;01(C3):341-6.
15. Jang DH, Kim WJ. Warm Temperature Deformation Behavior and Processing Maps of 5182 and 7075 Aluminum Alloy Sheets with Fine Grains. *Metals and Materials International*. 2018;24(3):455-63.
16. Kaibyshev R, Malopheyev S. Mechanisms of Dynamic Recrystallization in Aluminum Alloys. *Materials Science Forum*. 2014;794-796:784-9.

Table 1 Composition of the 5182 aluminium alloy in wt%

	Si	Fe	Cu	Mn	Mg	Cr	Zn	Ti
Specification limits	0.20	0.35	0.15	0.20- 0.50	4.0- 5.0	0.10	0.25	0.10
Alloy used	0.103	0.223	0.089	0.456	4.89	0.039	NA*	0.008

* NA – not analysed

Table 2 Optimal weld process parameters used in reference 8 for high and low speed FSW of 5182-H111 plate

	Forging Force (kN)	Feed Rate (m/min)	Feed Rate (mm/s)	Tool Speed (rev/min)	Weld Pitch (mm/rev)	Peak Pin Temp (°C)
Low Speed	27	0.2	3.33	500	0.4	543
High Speed	59	1.5	25.0	500	3.0	505

Table 3 Mechanical property data for the 5182-H111 alloy and the low and high speed welds

	UTS (MPa)	0.2% Proof Strength (MPa)	Elongation at Failure (%)	Tensile Joint Efficiency
Low speed	311	153	29.0	1.03
High speed	316	177	25.4	1.04
Parent alloy	302	145	27.8	-

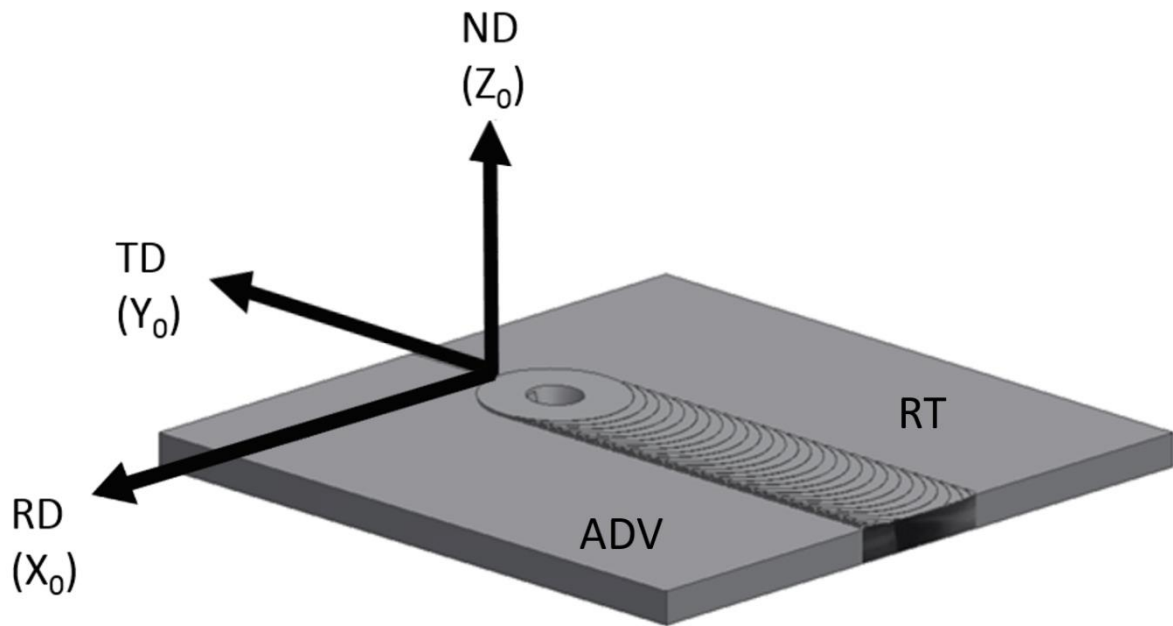


Figure 1 Sample and axis orientation used in the EBSD analysis. ADV denotes the advancing side of the weld and RT the retreating side.

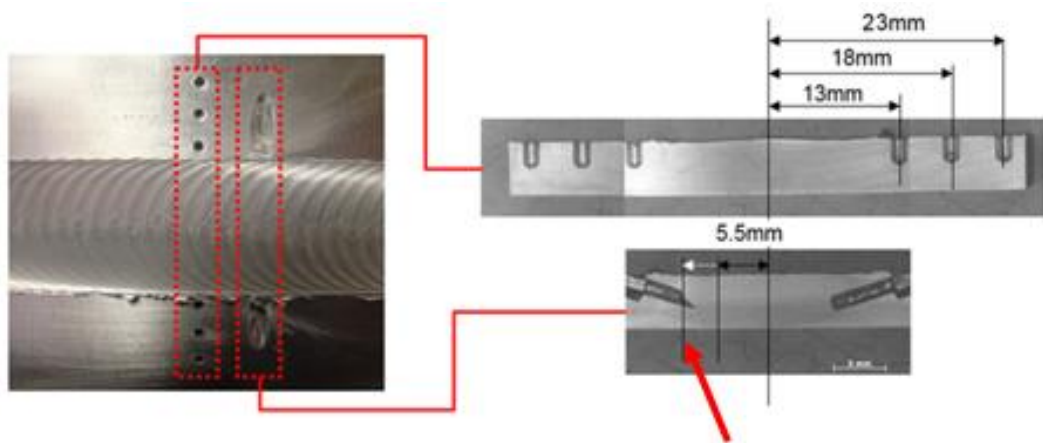
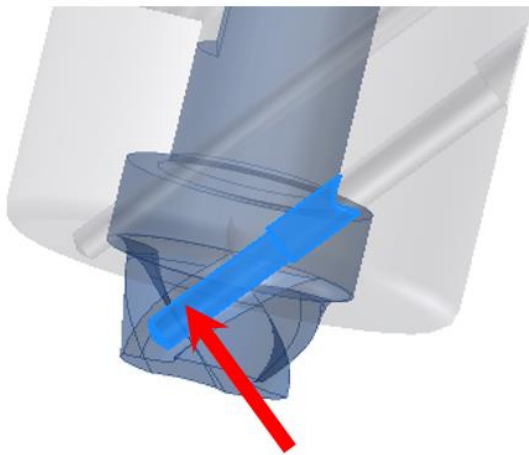


Figure 2a Thermocouple positions in the 5182 plates; the tips of the thermocouples are all at mid-thickness. The red arrow indicates the thermomechanically induced displacement of the thermocouples initially placed at 5.5 mm.



Figure 2b FS butt weld in 5182-H11 plate showing the thermocouple positions.



Thermocouple Hole

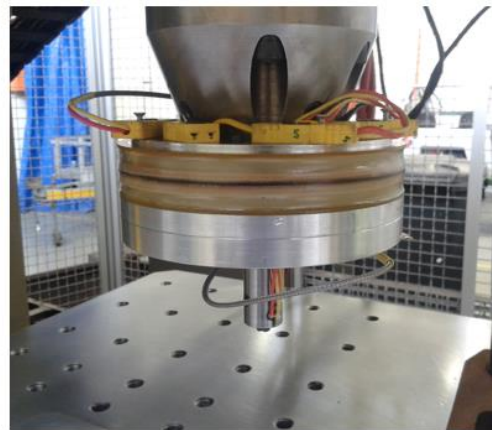


Figure 2c Illustration of the thermocouple embedded within the pin of the rotating tool, and an image of the tool with the telemetry system in place.

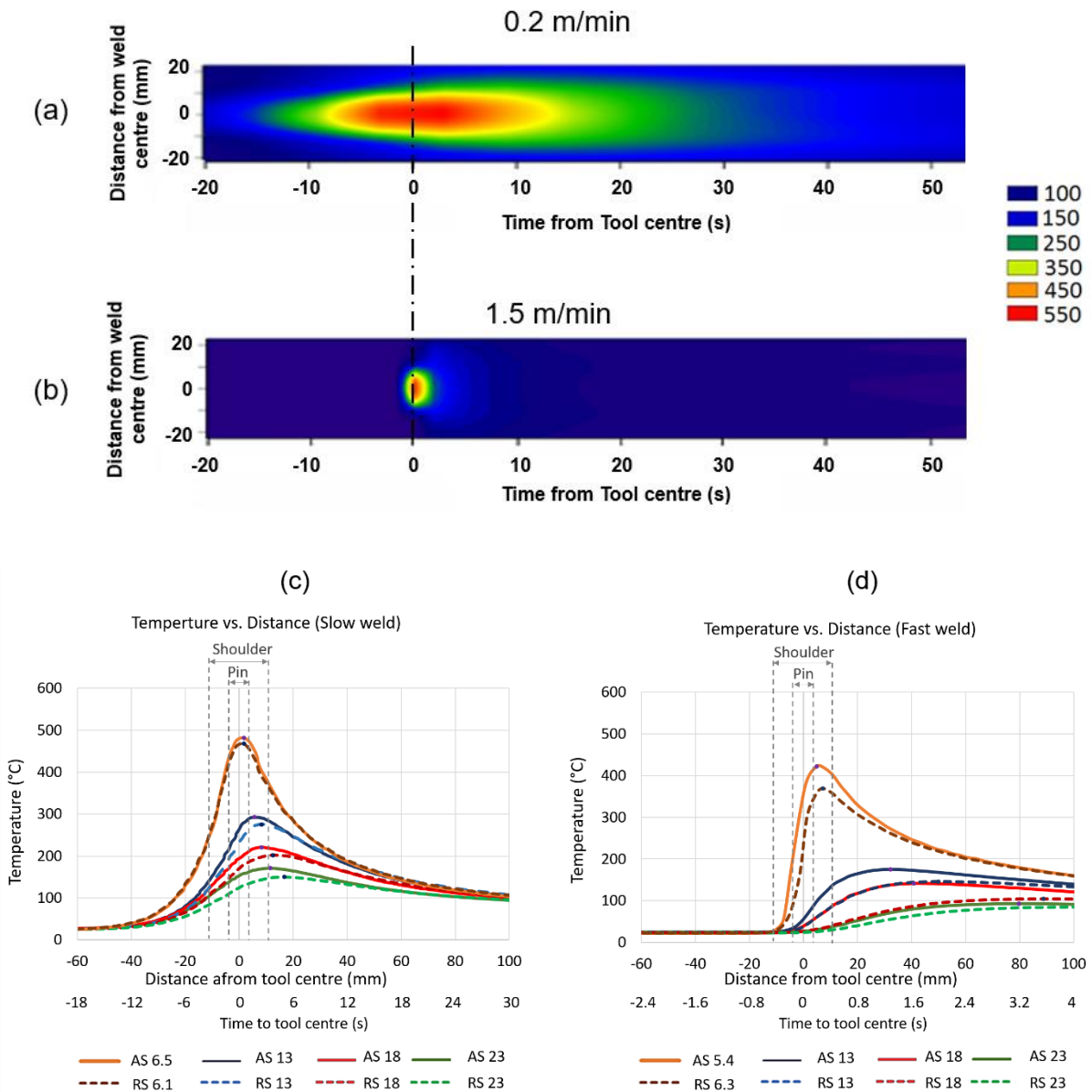


Figure 3 Temperature contour plots showing transverse thermal extent and time at temperature for a) FS welds made at 0.2 m/min (3.33 mm/s) and b) FS welds made at 1.5 m/min (25 mm/s). c) and d) Temperature measurements as a function of the transverse distance from the tool centreline, with negative distances representing distance ahead of the tool.

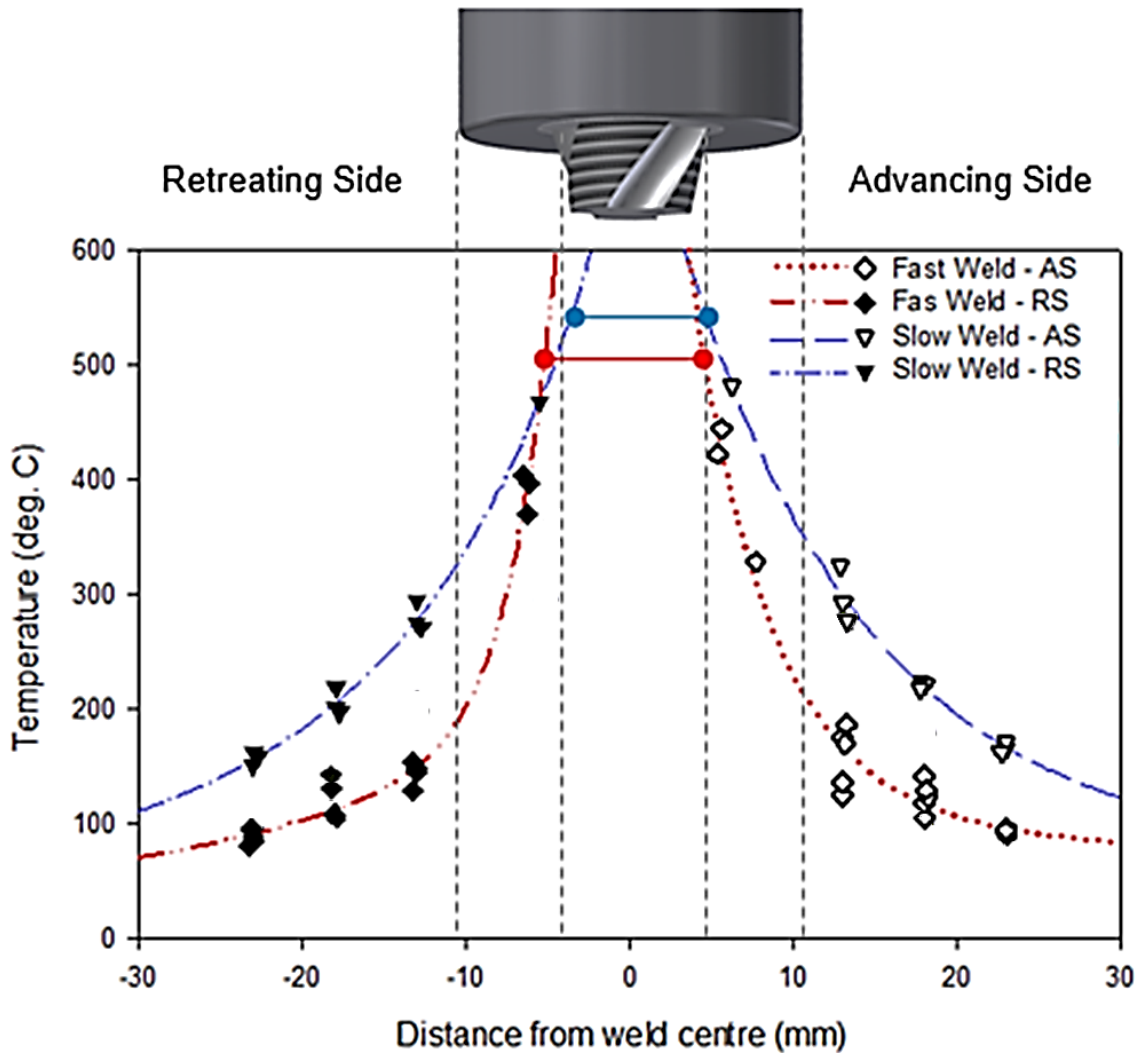


Figure 4 Peak temperature measurements recorded at the various thermocouple positions during passage of the tool for the butt weld specimens. Negative distances represent the retreating side while positive distances correspond with the advancing side. The blue and red dots denote the peak temperatures measured within the tool pin for the 0.2 m/min and 1.5 m/min welds respectively.

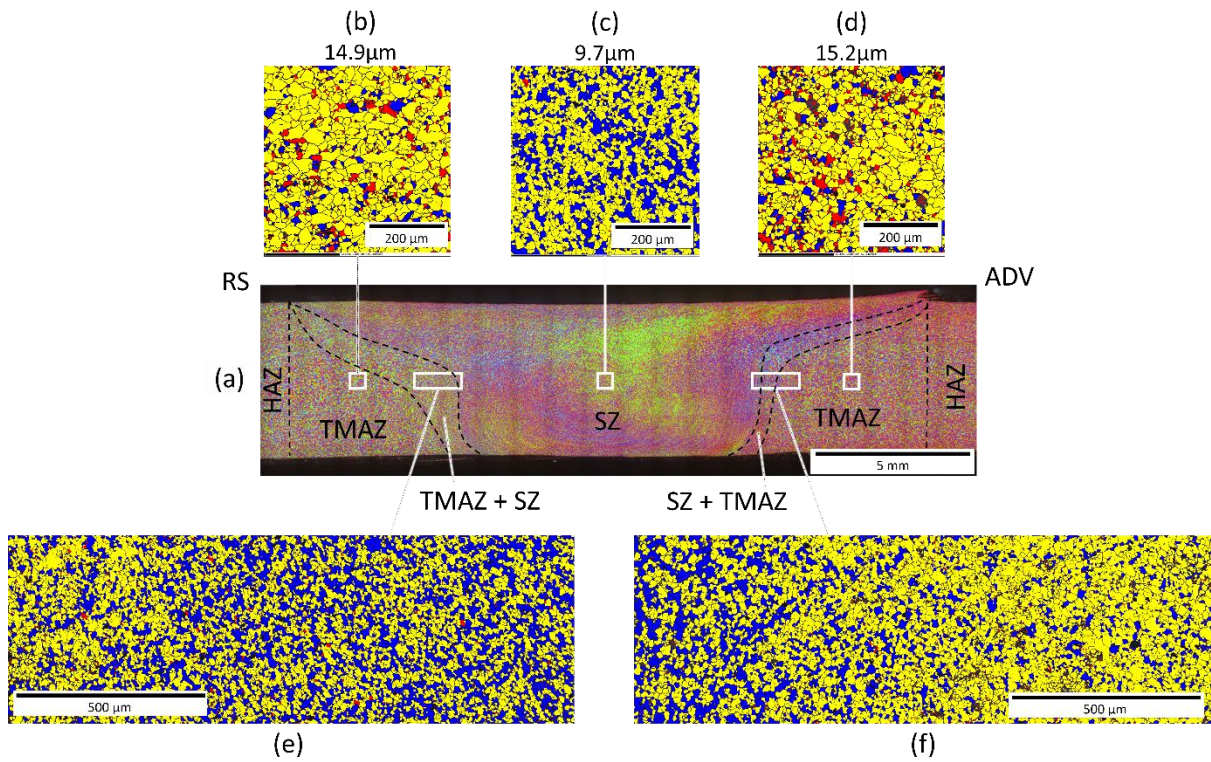


Figure 5 (a) Polarised light micrograph of the 0.2 m/min weld. (b) to (f) present the EBSD recrystallized fraction plots (GAM) for the areas indicated. Blue ($<1^\circ$ average misorientation) represents recrystallized grains, yellow ($1^\circ - 7.5^\circ$) are substructured, and red ($>7.5^\circ$) is deformed.

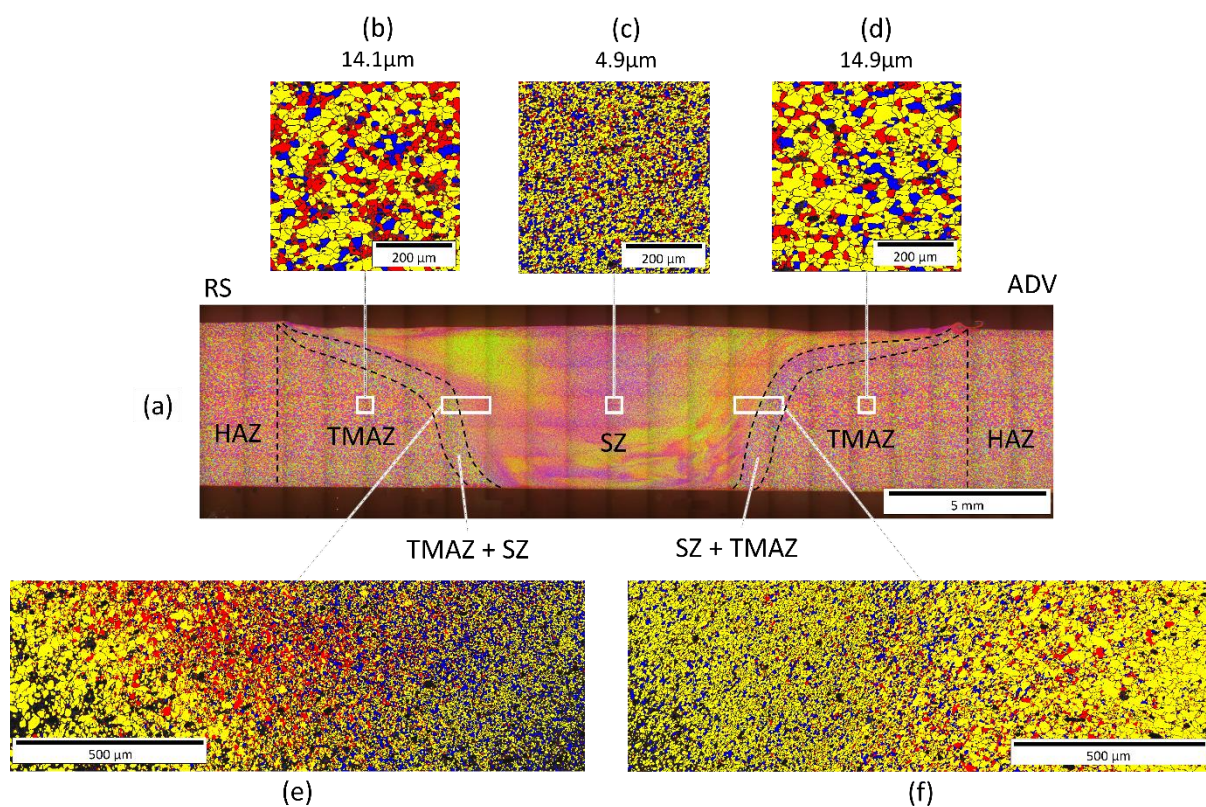


Figure 6 (a) Polarised light micrograph of the 1.5 m/min weld. (b) to (f) present the EBSD recrystallized fraction plots for the areas indicated. Blue ($<1^\circ$ average misorientation) represents recrystallized grains, yellow ($1^\circ - 7.5^\circ$) are substructured, and red ($>7.5^\circ$) is deformed.

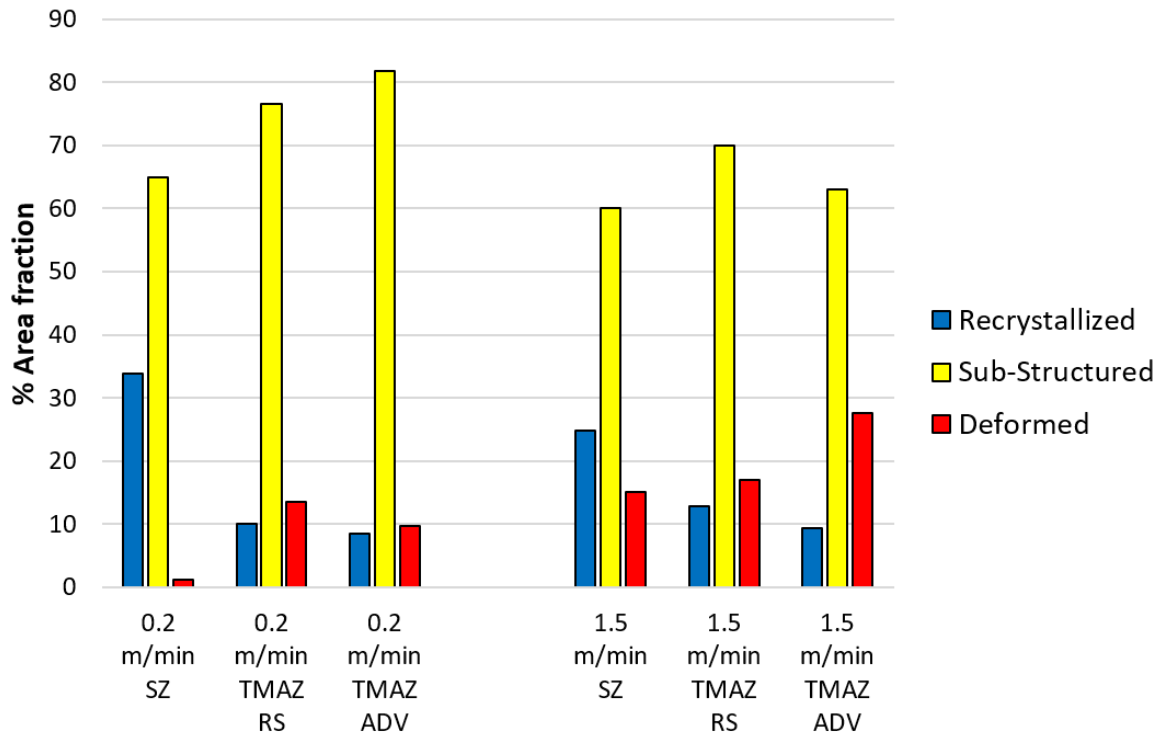


Figure 7 Recrystallized fraction component (GAM area fraction) for recrystallized, substructured and deformed gains in the SZ and HAZ of the 0.2 m/min and 1.5 m/min welds.

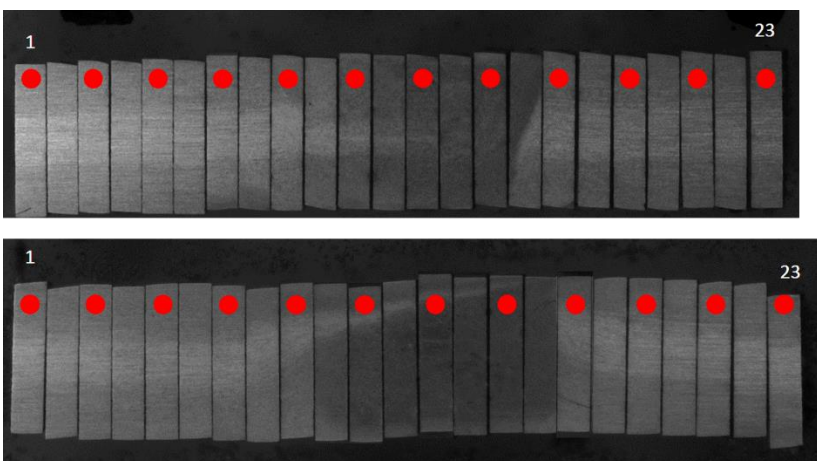
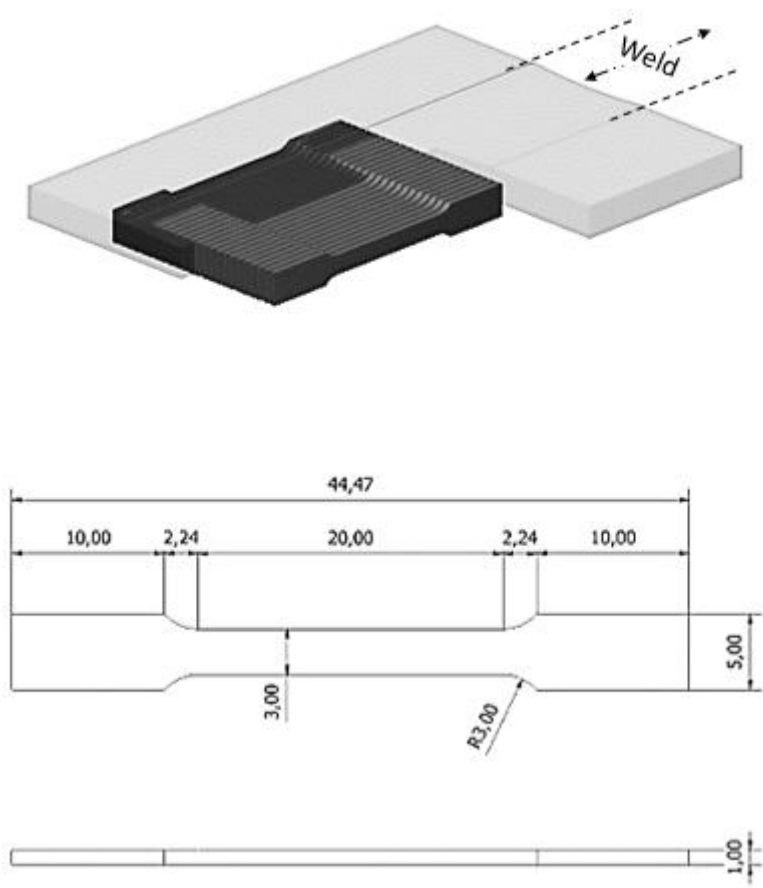


Figure 8 Locations where tensile samples were sectioned from the weld. Samples were machined from the parent material and across the weld zone.

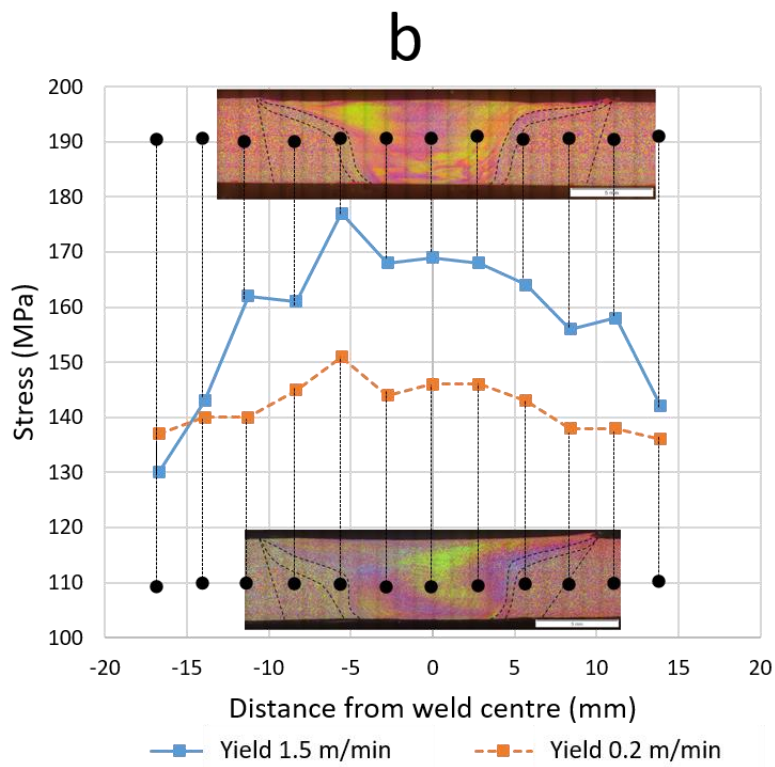
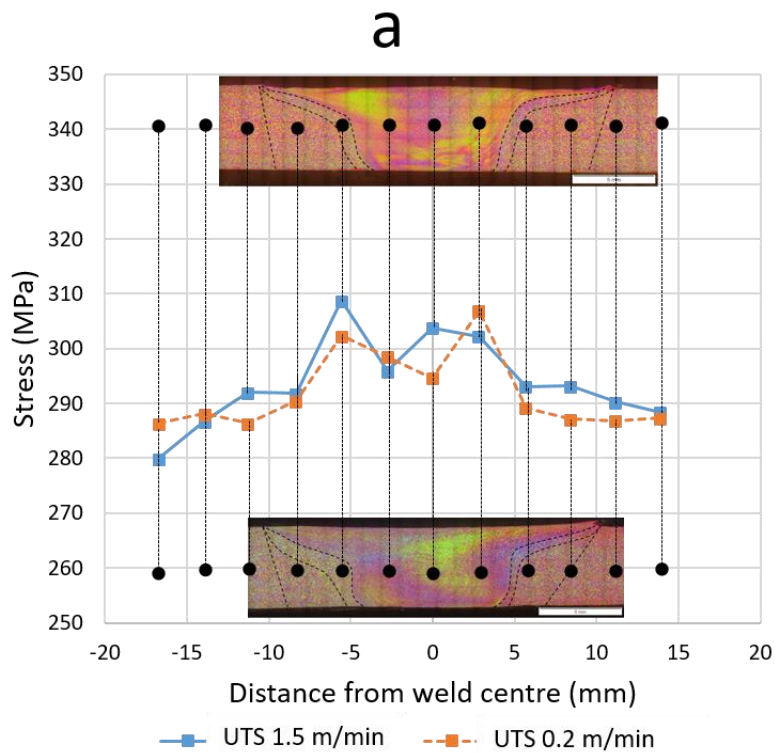


Figure 9 Results of small section tensile specimens: (a) UTS (b) yield strength as a function of position across the weld, with the macrographs scaled and positioned correctly in terms of sample removal.

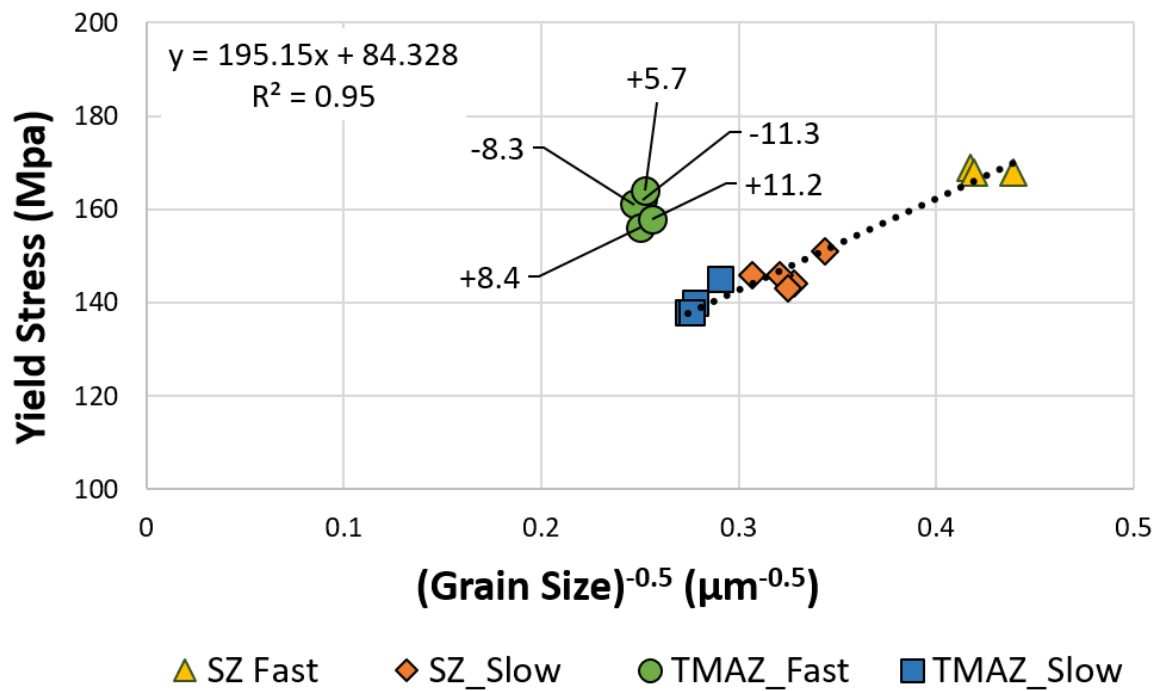


Figure 10 Hall-Petch relationship for yield strength of the 0.2 m/min (slow) weld and 1.5 m/min (fast) weld. The numbers given for the fast weld data represent distance relative to weld centreline.

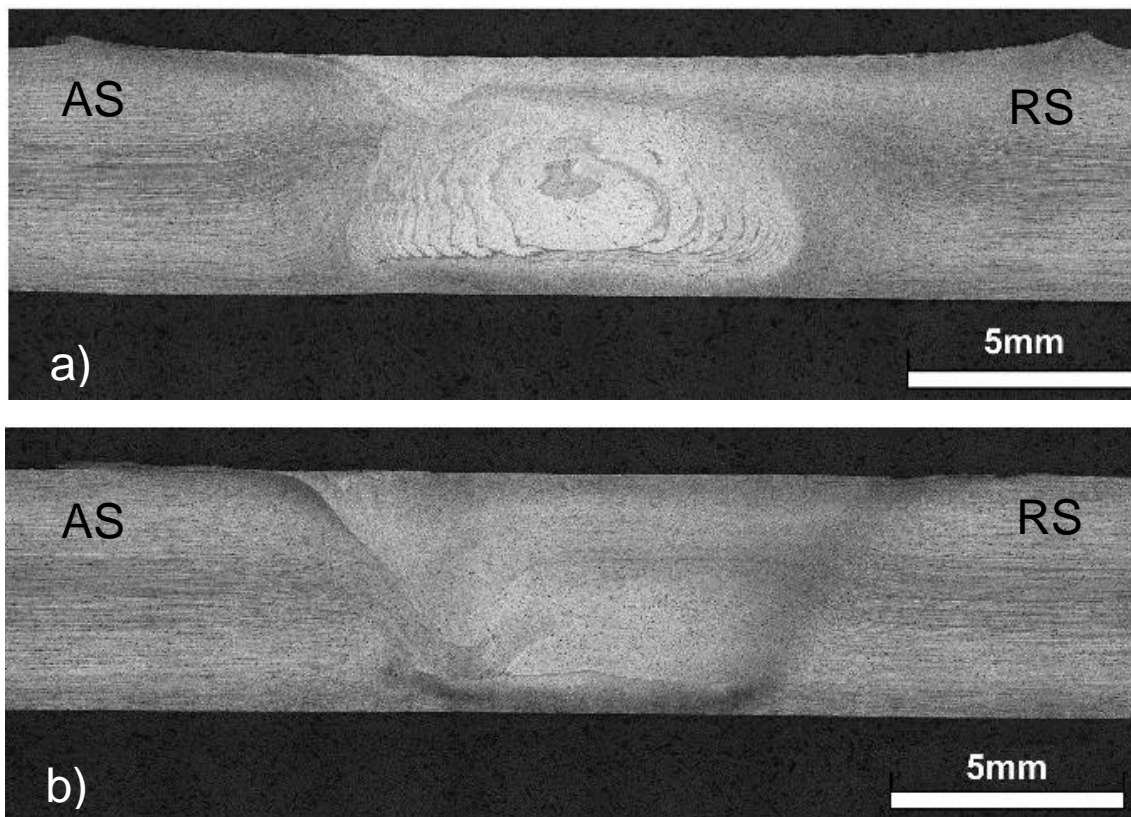


Figure 11 Macrographs of weld cross-section a) Welding speed 0.2 m/min.
b) Welding speed 1.5 m/min. AS indicates the advancing side of the weld and RS the retreating side.

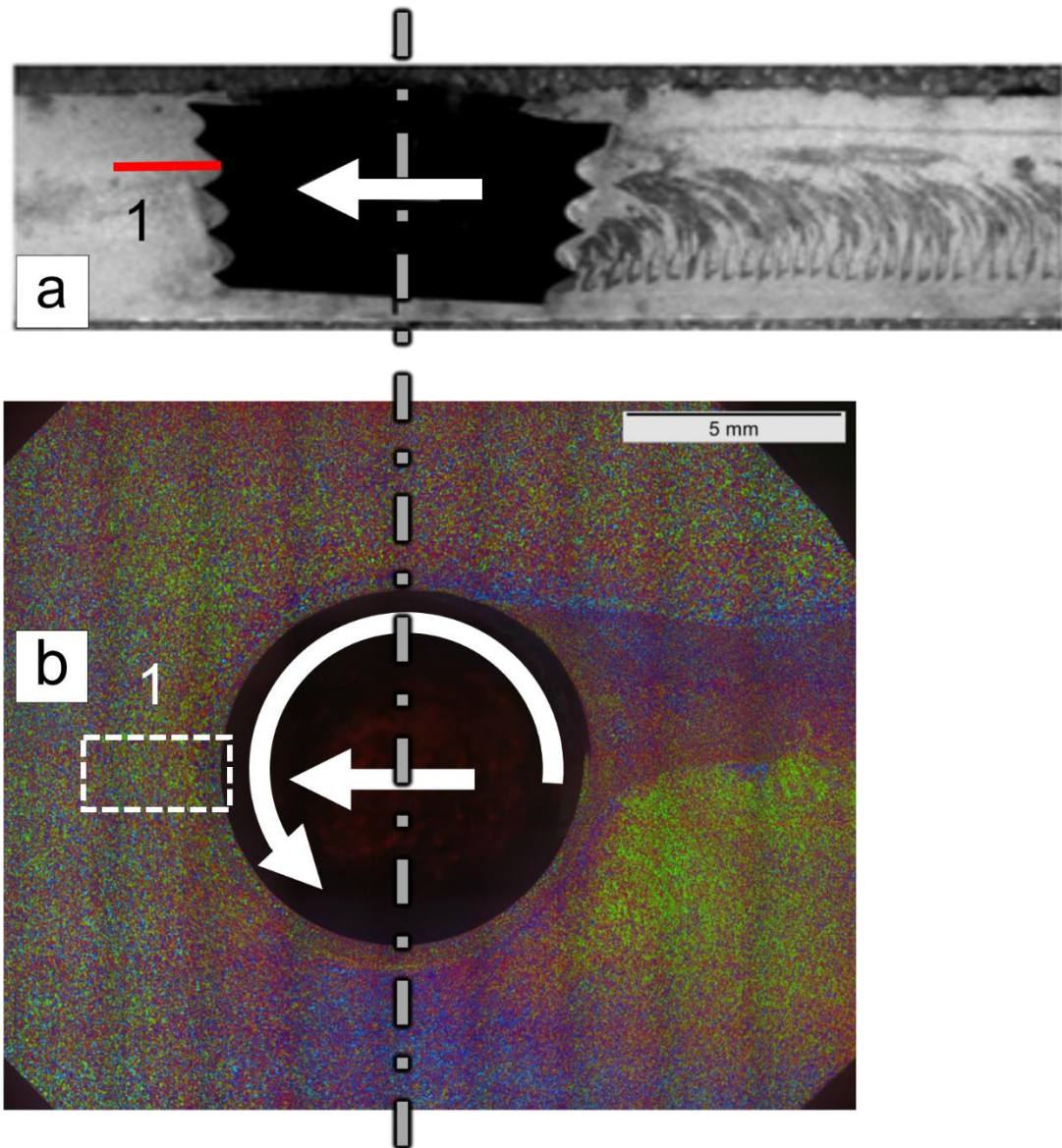


Figure 12 a) Section through the centre of the pin for a pin-break weld made at 0.2 m/min; b) Polarised light macrograph showing the plane 1.7 mm below the surface of the weld. The red line in (a) and the rectangular area in (b) denoted by the numeral "1", illustrate the area that was investigated by EBSD.

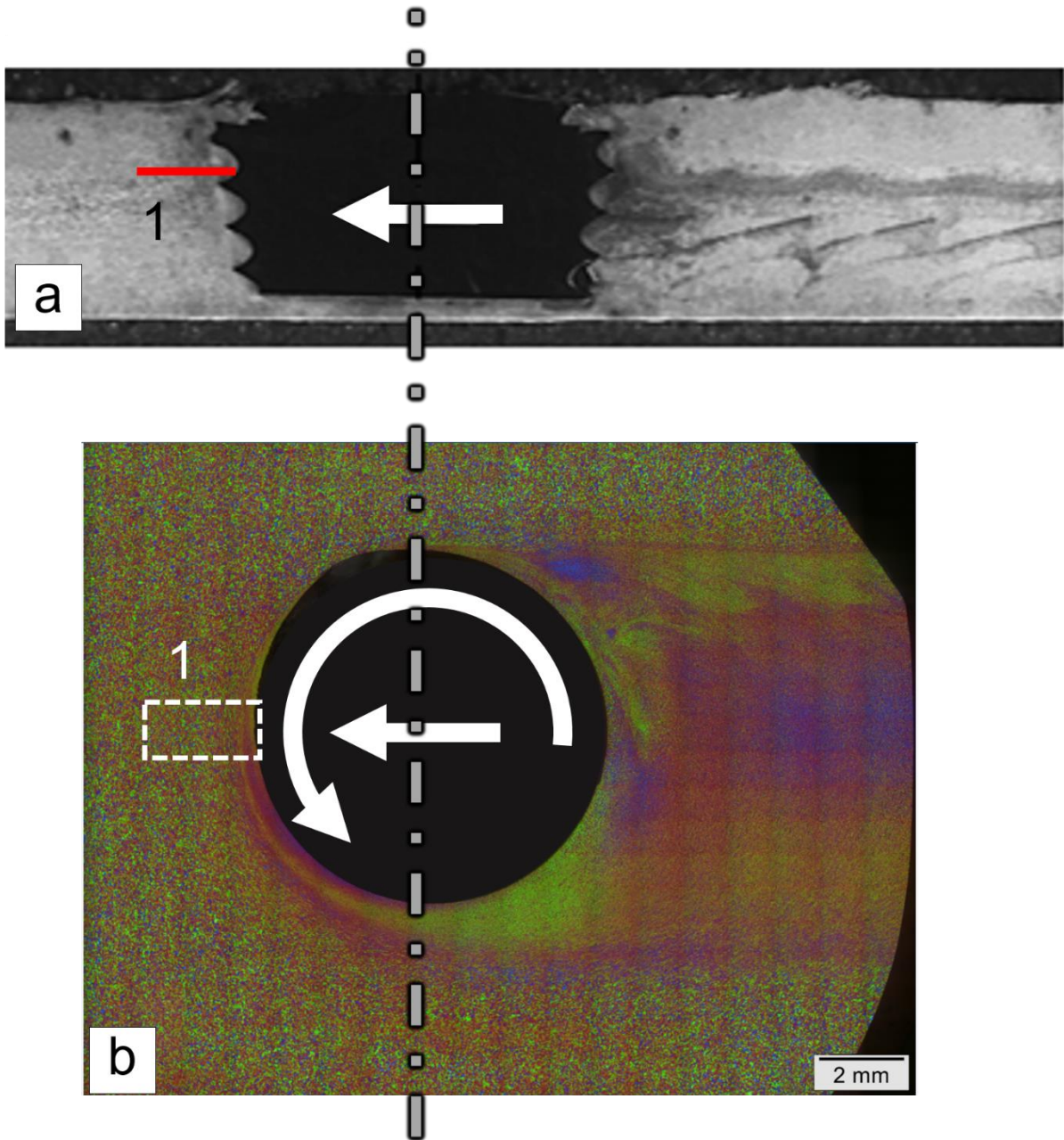


Figure 13 a) Section through the centre of the pin for a pin-break weld made at 1.5 m/min; b) Polarised light macrograph showing the plane 1.7 mm below the surface of the weld. The red line in (a) and the rectangular area in (b) denoted by the numeral “1”, illustrate the plane that was investigated by EBSD.

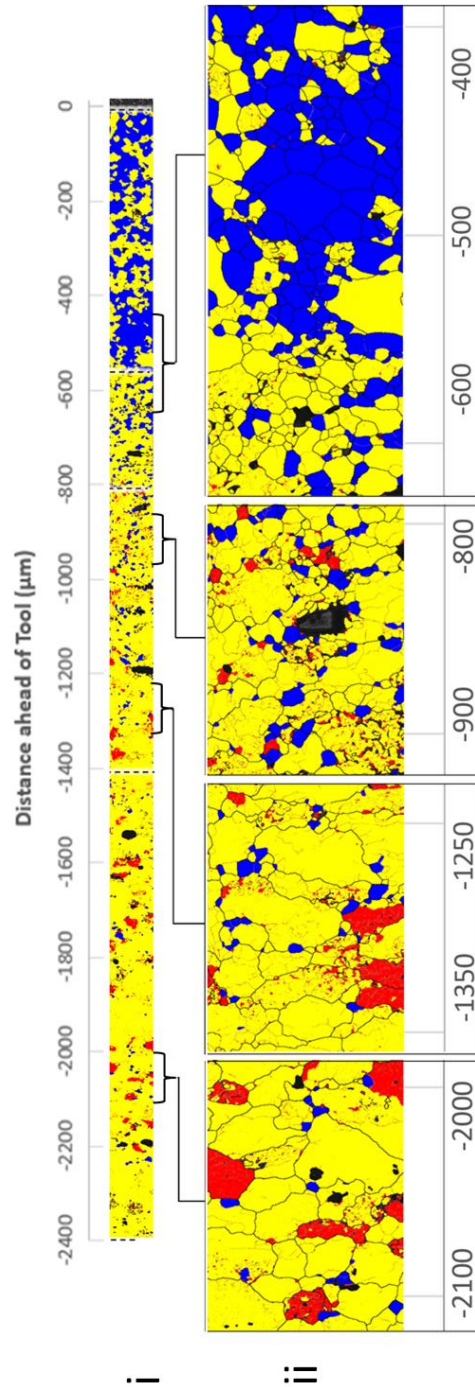


Figure 14 Recrystallized fraction plot in the TD-RD plane ahead of the tool pin of region 'a' in Figure 12 for the 0.2 m/min weld. Recrystallized grains (misorientation $<1^\circ$) are shown in blue, moderately strained grains (misorientation 1° - 7.5°) in yellow, and highly strained grains (misorientation $>7.5^\circ$) in red. The images in row ii shows higher magnification views of selected regions from that in row i.

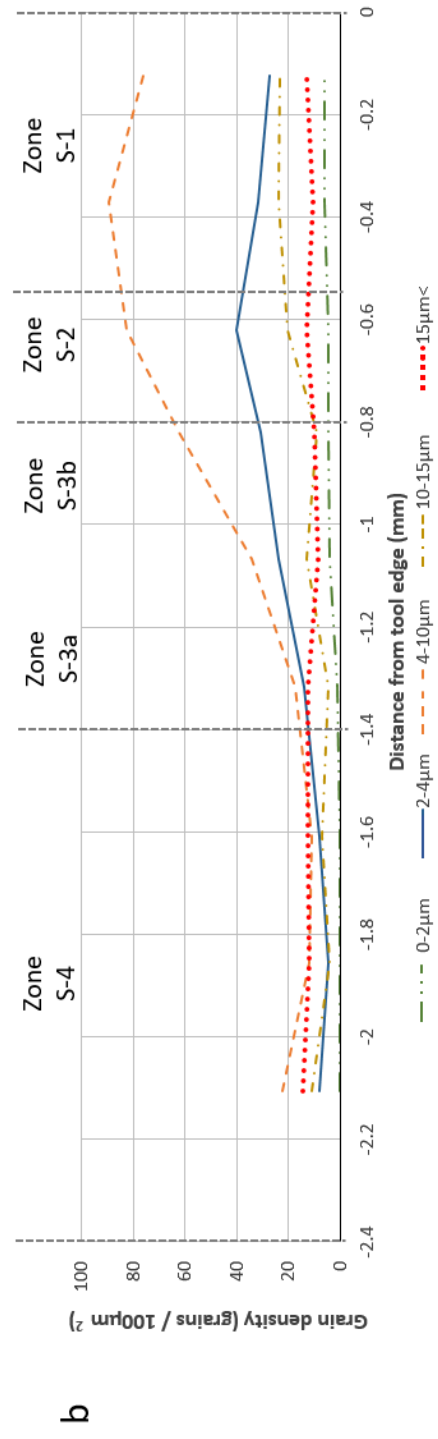
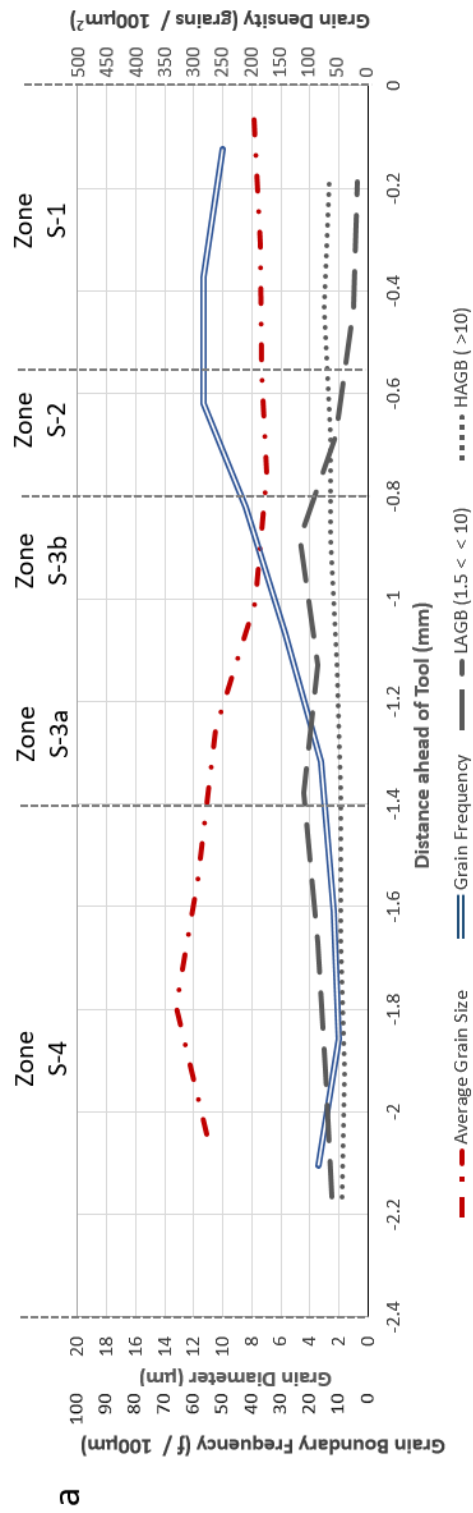


Figure 15 EBSD data for the slow speed weld showing: a) Grain boundary frequency as a function of distance ahead of the tool pin and b) Grain density as a function of distance ahead of the tool pin for grain sizes ranges of 0-2 µm, 2-4 µm, 4-10 µm and >15 µm.

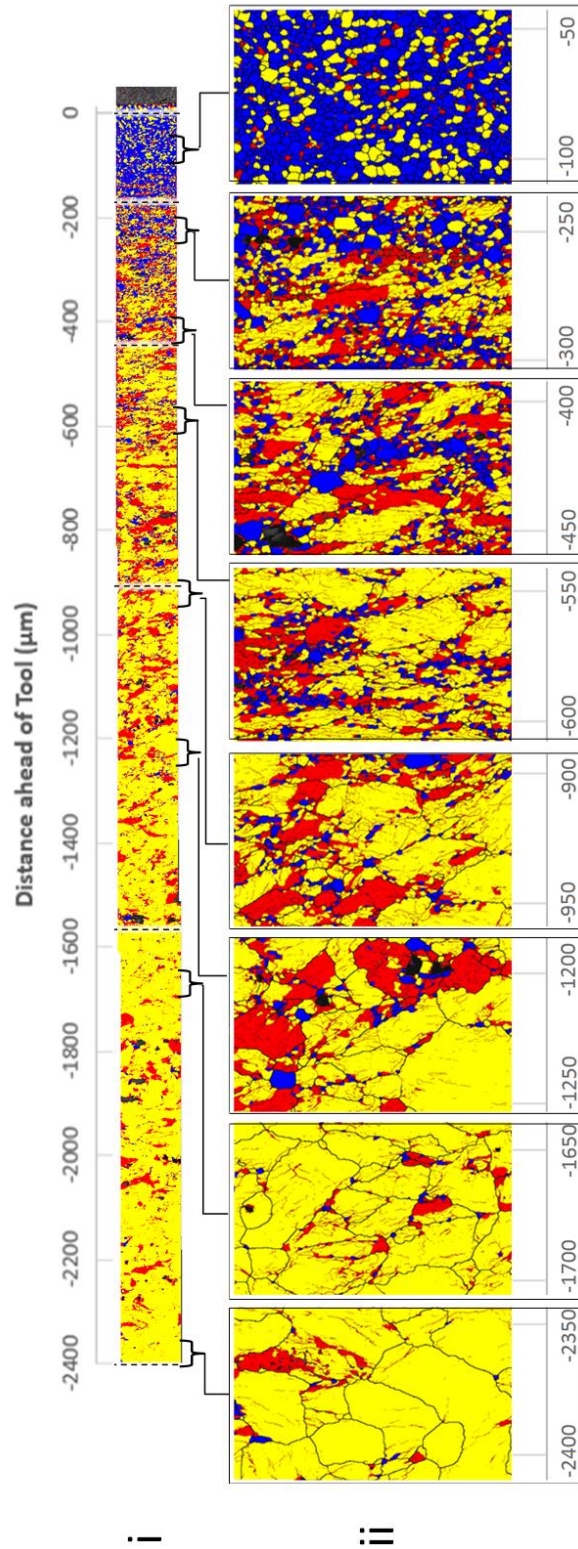


Figure 16 Recrystallized fraction plot in the TD-RD plane ahead of the tool pin of region 'a' in Figure 12 for the 1.5 m/min weld. Recrystallized grains (misorientation $<1^\circ$) are shown in blue, moderately strained grains (misorientation 1° - 7.5°) in yellow, and highly strained grains (misorientation $>7.5^\circ$) in red. The images in row ii shows higher magnification views of selected regions from that in row i.

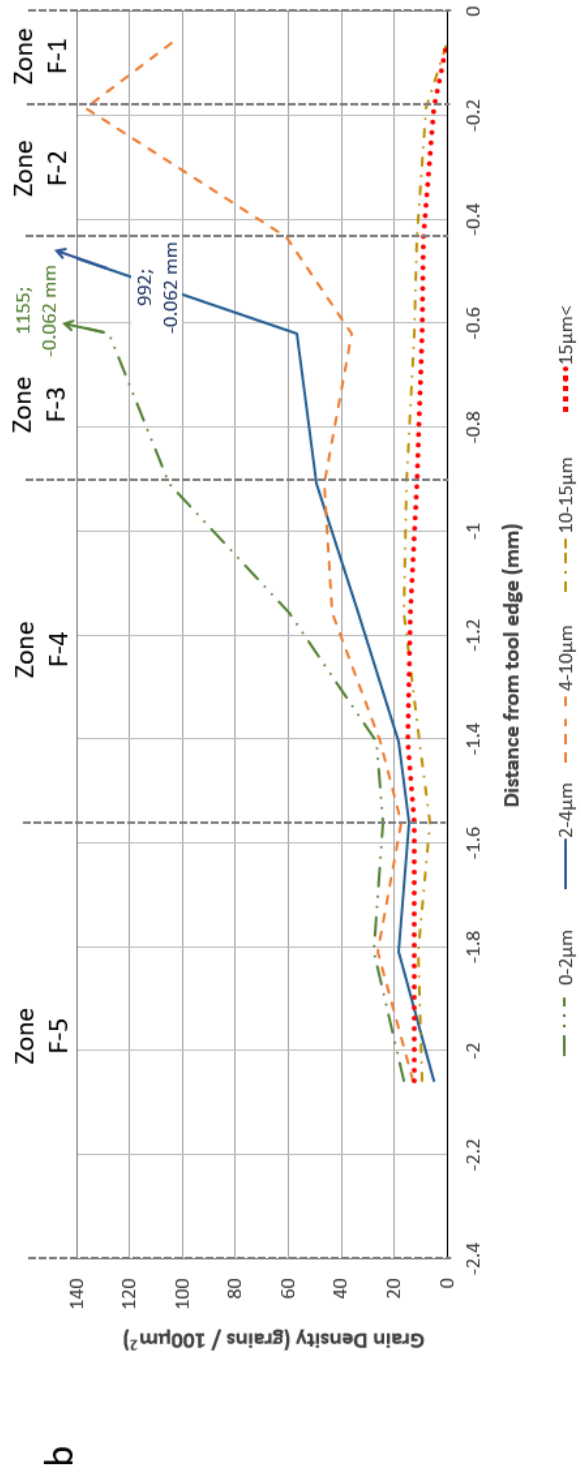
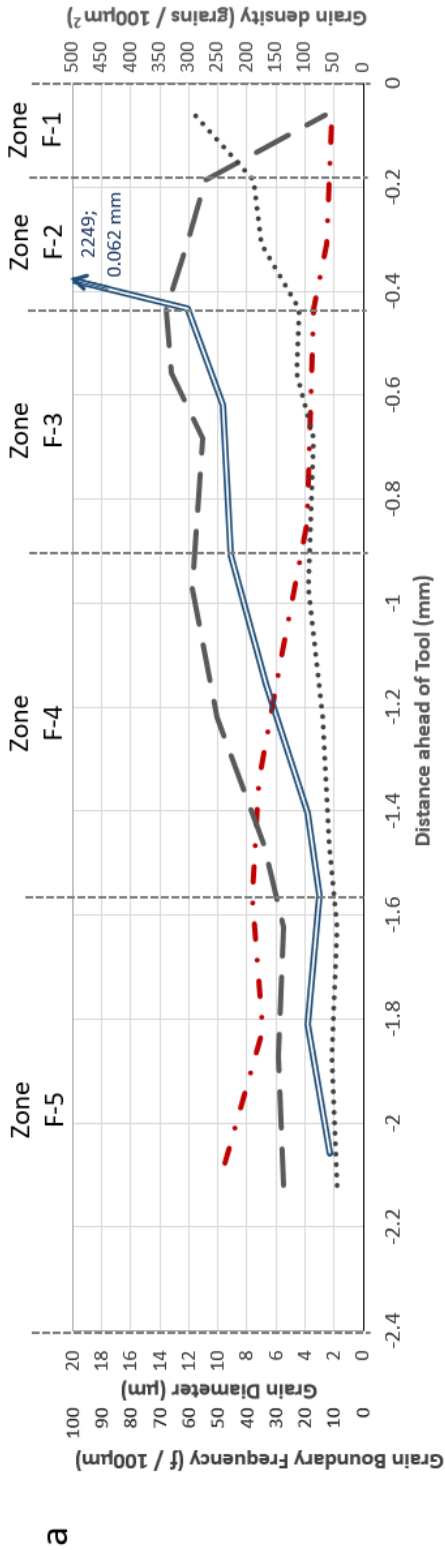


Figure 17 EBSD data for the high speed weld showing: a) Grain boundary frequency as a function of distance ahead of the tool pin and b) Grain density as a function of distance ahead of the tool pin for grain size ranges of 0-2 µm, 2-4 µm, 4-10 µm and >15 µm.

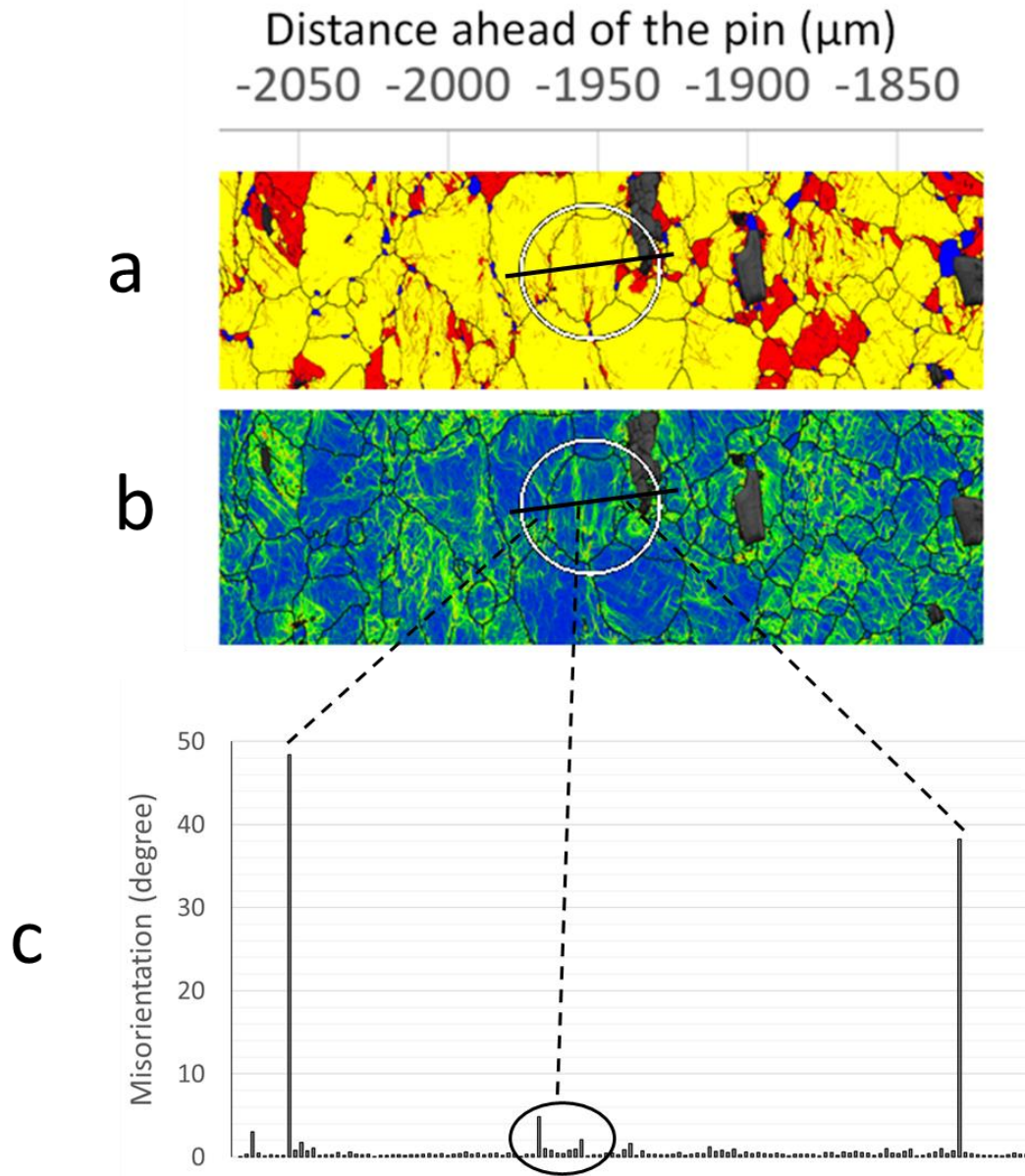


Figure 18 Misorientation data for a grain approximately 2 mm ahead of the tool pin undergoing geometric dynamic recrystallisation. (a) represents the recrystallized fraction plot where recrystallized grains (misorientation $<1^\circ$) are shown in blue, moderately strained grains (misorientation 1° - 7.5°) in yellow, and highly strained grains (misorientation $>7.5^\circ$) in red. (b) Presents the local misorientation plot (kernel average misorientation), and (c) presents the misorientation in degrees, measured across the grain along the solid black line, that is orientated almost perpendicular to the welding direction.